Modulation of the Convectively Coupled Kelvin Waves over South America and the Tropical Atlantic Ocean in Association with the Madden–Julian Oscillation

YANJUAN GUO AND XIANAN JIANG

Joint Institute for Regional Earth System Science and Engineering, University of California, Los Angeles, Los Angeles, California

DUANE E. WALISER

Joint Institute for Regional Earth System Science and Engineering, University of California, Los Angeles, Los Angeles, and Jet Propulsion Laboratory, California Institute of Technology, Pasadena, California

(Manuscript received 15 July 2013, in final form 3 November 2013)

ABSTRACT

In this study, evidence of the strong modulation of the convectively coupled Kelvin wave (CCKW) activity by the Madden–Julian oscillation (MJO) is presented, with a particular focus over the South America and tropical Atlantic region. The MJO impacts on CCKWs over this region, as noted in anomalous fields of rainfall as well as vertical profiles of wind, moisture, and temperature, are primarily through the modulation of Kelvin wave amplitude, with secondary effects on vertical structure, and little impact on wavenumber. CCKW activity is enhanced during MJO phases 8, 1, and 2 and damped during MJO phases 4, 5, and 6.

Further analyses reveal that the strong modulation of the MJO on the CCKW activity could be largely through two factors: namely, the vertical zonal wind shear and the lower- to middle-tropospheric specific humidity. The CCKW activity tends to be enhanced during MJO phases when the easterly vertical wind shear and positive low- to midtroposphere moisture anomalies are present and vice versa. These two physical processes associated with the MJO are found to have positively (negatively) reinforcing influences on the CCKW activity in phase 1 (4 and 5), while counteracting influences in phases 2, 3, 6, 7, and 8, leading to the observed MJO cycle of the CCKW activity anomalies in the study region. The results presented in this study may have important implications for extended-range prediction of tropical wave activity and might suggest possible roles of the upstream CCKWs in the initiation of the MJO in the western Indian Ocean.

1. Introduction

Deep convection in the tropics is observed to be organized in part by a hierarchy of zonally propagating wavelike disturbances with a broad spectrum in both space and time (Nakazawa 1988). These tropical modes constitute a major fraction of the tropical convective variability (e.g., Takayabu 1994; Wheeler and Kiladis 1999, hereafter WK99; Kiladis et al. 2009). Among them, the Madden–Julian oscillation (MJO) has received extensive attention since its discovery in the early 1970s (Madden and Julian 1971, 1972). The MJO is the dominant mode of tropical intraseasonal (30–90 day) variability that is characterized by slow ($\sim 5\,\mathrm{m\,s^{-1}}$) and global-scale eastward propagation of convection anomalies (e.g., Zhang 2005). Another important eastward-propagating mode is the convectively coupled equatorial Kelvin wave (CCKW; e.g., Takayabu and Murakami 1991; Takayabu 1994; Dunkerton and Crum 1995; WK99; Wheeler et al. 2000; Roundy 2008), which features higher frequency and smaller spatial scales compared to the MJO.

Ever since its discovery, aspects of the MJO have been compared to the Kelvin wave because of a number of characteristics that they appear to have in common. Early theories for the MJO portrayed it as an equatorial Kelvin wave whose properties were modified by the coupling between the convection and large-scale circulation (e.g., Emanuel 1987; Wang 1988), and many marginally successful models for the MJO were based on moist Kelvin wave dynamics (e.g., Chang and Lim 1988; Cho et al. 1994). However, more recent studies suggest that the

Corresponding author address: Dr. Yanjuan Guo, Jet Propulsion Laboratory, M/S 233-304, 4800 Oak Grove Drive, Pasadena, CA 91109.
E-mail: yguo@jifresse.ucla.edu

DOI: 10.1175/JAS-D-13-0215.1

MJO and the Kelvin waves behave differently in many respects. For example, wavenumber–frequency analyses show that the MJO and the CCKWs occupy distinct domains of the spectrum (WK99). Also, examination of the relationship between surface pressure and low-level zonal winds reveals that westerlies are coincident with high pressure in a Kelvin wave, while the opposite is more nearly true for the MJO (Roundy 2012). Despite the recent consensus that the MJO is a fundamentally different mode from a Kelvin wave, it is still not completely clear whether they are two distinct elements in the spectrum of eastward-propagation signals or whether there exists a continuous spectrum with hybrid (Roundy 2012) or transitional (Sobel and Kim 2012) signals in between.

Several studies have suggested that the MJO modulates the CCKWs over different geographical locations. Roundy (2008) composited the CCKWs over the tropical Indian Ocean during active and suppressed MJO events and found that the CCKW convection is enhanced (decreased) during the active (suppressed) MJO events, with the enhanced (decreased) CCKW convection mainly confined within the envelopes of the active (suppressed) MJO convection. Ventrice et al. (2012b) noticed that the strongest CCKWs propagating over the tropical Atlantic region are commonly associated with the decay of the active convective signal of the MJO over the Pacific and eastward propagation over the Western Hemisphere. This result is also consistent with previous findings by Straub and Kiladis (2003a) and Mekonnen et al. (2008), in which the strong CCKWs over the eastern Pacific and Africa are found to be commonly associated with the demise of the MJO convective signature over the Pacific. In this work, we will investigate the MJO modulation of the CCKWs over the South America and tropical Atlantic region where considerable CCKWs variance exists. A recent study by Liebmann et al. (2009) suggested that a substantial fraction of CCKWs over this region results from preexisting Kelvin waves over the eastern Pacific Ocean, while another fraction of them are forced by disturbances propagating equatorward from central and southern South America. This region is of particular interest for the following reasons: First, as will be shown in section 3, both the climatological and the MJO composite CCKW convection variance over this region exhibit a local peak value with a magnitude comparable to that in the western Pacific warm pool region. Second, the modulation of CCKWs by the MJO over this specific region has not been studied in detail. For example, the study of Roundy (2008) was focused on the tropical Indian Ocean, while Straub and Kiladis (2003a) and Mekonnen et al. (2008) focused on the eastern Pacific and Africa. Although Ventrice et al. (2012b) did look at the relationship between the MJO and the CCKW over the tropical Atlantic, the analysis was carried out at a rather basic level since that was not the focus of that paper. Thus, a close examination of the MJO modulation of the CCKWs over the South America and tropical Atlantic region is desirable.

Moreover, with further research, this line of inquiry could lead to better understanding and prediction of the modulation of even higher-frequency disturbances as well as the subsequent activity over Africa and the Indian Ocean, the latter possibly being important to MJO initiation. For example, Liebmann et al. (2011) revealed that Kelvin waves act as a precursor of extreme precipitation events in northeastern Brazil. Ventrice et al. (2012a,b) found that CCKWs can impact Atlantic tropical cyclogenesis through both the convection and the large-scale circulation anomalies associated with them. Other influences by the CCKWs on the variations of the Atlantic intertropical convergence zone (ITCZ) (Wang and Fu 2007), the West African monsoon (Mounier et al. 2007), convective precipitation in eastern Africa (Mekonnen et al. 2008) and Maritime Continent (Ridout and Flatau 2011), and mesoscale organization over central Africa (Nguyen and Duvel 2008) have also been noticed. Thus, improved understanding of the relationship between the MJO and the CCKWs over this region could lead to improved prediction of these phenomena on the intraseasonal time scale. Although our current effort will be focused on the modulation of the MJO on the CCKW solely, the relation between the MJO and other types of convectively coupled equatorial waves, such as the equatorial Rossby waves, mixed Rossby gravity waves, and inertio-gravity waves, is very important to investigate and characterize, relevant to both theoretical and practical forecasting concerns. These will be addressed in a future study.

The rest of this paper is organized as follows. The next section briefly describes the data and methodology used in this paper. Section 3 then discusses detailed characteristics of the CCKWs over South America and the tropical Atlantic Ocean during different MJO phases. In section 4, we will examine a number of physical factors through which the MJO appears to modulate the CCKWs. Finally, the main conclusions and a discussion are presented in section 5.

2. Data and methodology

a. Data

In this study, daily rainfall data from the Tropical Rainfall Measuring Mission (TRMM) 3B42 version 7 dataset (Huffman et al. 2007) as a proxy of the tropical deep convection are used to identify the MJO and the

CCKW events. The method to extract the convection signals corresponding to these two modes will be introduced in section 2b. To examine the dynamical and thermodynamical characteristics associated with the MJO and Kelvin wave, daily atmospheric variables (temperature, winds, specific humidity, etc.) from the Interim European Centre for Medium-Range Weather Forecasting (ECMWF) Re-Analysis (ERA-Interim) dataset (Dee et al. 2011) are used. Reanalysis data at 12 vertical levels between 1000 and 100 hPa are used: 1000, 925, 850, 700, 600, 500, 400, 300, 250, 200, 150, and 100 hPa. Both TRMM rainfall and ERA-Interim data are interpolated onto a horizontal resolution of 2.5° × 2.5° from their original resolutions (1° × 1° for TRMM, and 1.5° × 1.5° for ERA-Interim), and the time period covers from 1 January 1998 to 30 April 2012.

The all-season real-time multivariate MJO (RMM) index developed by Wheeler and Hendon (2004) is used as a measure of the state of the MJO. The pair of daily RMM indices (RMM1 and RMM2) are obtained based on an empirical orthogonal function (EOF) analysis of the combined fields of equatorially averaged 850- and 200-hPa zonal wind and National Oceanic and Atmospheric Administration (NOAA) outgoing longwave radiation (OLR) and are used to indicate the MJO phase and amplitude on a particular day.

b. Methodology

To isolate the convection signals corresponding to the MJO or the CCKW, a zonal wavenumber–frequency filtering, or so-called WK filtering (WK99), is applied to the TRMM rainfall. This is accomplished by retaining only those spectral coefficients corresponding to the spectral peaks associated with a specific mode in the wavenumber–frequency domain. More details on the methodology can be found in WK99. In this study, the MJO filtering retains the coefficients corresponding to periods from 30 to 96 days and wavenumbers from 0 to 10. Here, positive wavenumbers correspond to eastward-propagating waves. For the Kelvin wave, eastward-propagating signals with periods from 2.5 to 15 days and wavenumbers from 1 to 14 are extracted together with additional constraints from two theoretical Kelvin wave dispersion curves with equivalent depths of 8 and 50 m. Both symmetric and asymmetric components about the equator are retained for the MJO and CCKW filtering. Note that in reality, the convection signal associated with the CCKW is no longer symmetric about the equator over some region of the tropics owing to the modification by its coupling to convection as well as possible alteration by the background meridional wind shear. Prior to the WK filtering, the annual cycle (mean and the first three harmonics) of a certain variable was first removed from its daily time series to produce the anomalies at each grid point. These anomalies are then used to carry out the WK filtering, and the resulting anomalies are called MJO-filtered anomalies for the MJO-filtering or the Kelvin-filtered anomalies for the Kelvin filtering.

An MJO-cycle composite of a field is obtained by averaging this field over each of the eight MJO phases according to the RMM index. In this study, only "strong" MJO events (defined as $\mathrm{RMM1}^2 + \mathrm{RMM2}^2 \geq 1$) are used. Furthermore, this study focuses on the Northern Hemisphere extended winter season (November–April) when the traditionally defined MJO is most evident and coincident with the near-equatorial region (e.g., Waliser 2006).

3. Characteristics of CCKWs in the eight MJO phases

a. MJO cycle of the CCKW variance

In this section, the characteristics of CCKWs during different MJO phases will be analyzed in order to examine the modulation of CCKWs by the MJO. Before showing the CCKW variation with respect to the MJO phase, we first show the winter climatology of the MJO and CCKW activity indicated by the mean variances of the MJO- and Kelvin-filtered TRMM precipitation averaged over the 1998–2012 boreal winter seasons (December–April) (Fig. 1). The variance of the MJO-filtered precipitation is mostly confined to the eastern Indian Ocean and western Pacific warm pool region between 15°S and 10°N. Compared to the MJO, the CCKW variance is more globally distributed, occupying over almost the entire tropical region. In particular, a local peak with a comparable magnitude to that over the tropical Pacific is found over the South America and the tropical Atlantic, which is the region of focus of this paper. This is in contrast to the MJO, which exhibits a local maximum over this region but with a magnitude about a fifth of that over the warm pool. As with the MJO variance, there appears to be a close connection to the regions of large-scale convection and rising motion (i.e., ITCZ) and warmer SST, with the CCKWs being particularly pronounced over narrow ITCZ regions of the eastern Pacific and Atlantic Oceans. These overall features of the MJO and Kelvin wave variances based on TRMM rainfall are generally similar to previous studies based on OLR or brightness temperature data (e.g., WK99; Wheeler et al. 2000; Roundy and Frank 2004; Mekonnen et al. 2008; Kiladis et al. 2009).

Figure 2 shows the MJO modulation of the CCKW activity defined as the variance of the Kelvin-filtered TRMM precipitation. To highlight the intraseasonal

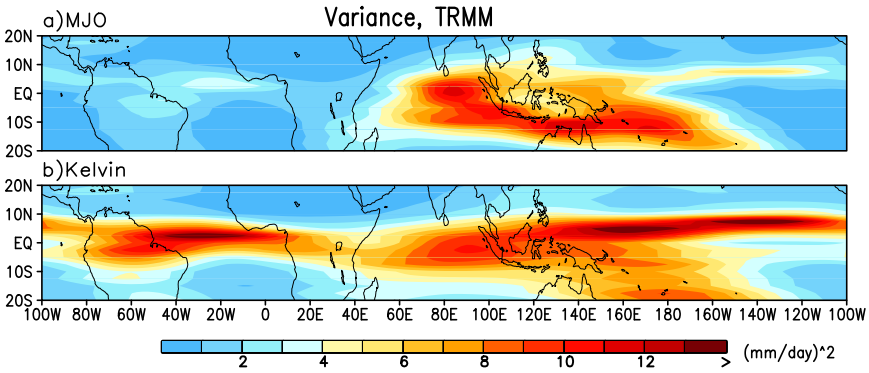

FIG. 1. Distribution of boreal winter (December–April)-mean variances of the (a) MJO- and (b) Kelvin-filtered TRMM precipitation ($mm^2\,day^{-2}$) during 1998–2012.

variability of the Kelvin wave activity, a 30–96-day temporal filtering is applied to the time series of the squared Kelvin-filtered rainfall anomalies before the composite. Only strong MJO days ($RMM1^2 + RMM2^2 \geq 1$) during the 1998–2012 boreal winter seasons are used for the MJO composite. The number of strong MJO days for each phase is indicated at the upper-right corner of each panel in Fig. 2. In Fig. 2, the composite MJO-filtered TRMM anomalies for each phase are also shown by black contours ($\pm 0.81\,mm\,day^{-1}$) to illustrate the locations of the MJO convection, which roughly correspond to ± 0.5 mean standard deviation of the rainfall anomalies averaged over the entire tropics (15°S–15°N, 0°–360°E) during the 1998–2012 winter seasons. It is found that overall the enhanced Kelvin wave activity is associated with the active MJO convection, while the reduced Kelvin wave activity is associated with the suppressed MJO convection. This is especially true for the region from the Indian Ocean to the eastern Pacific, which is consistent with previous findings by Roundy (2008). Nevertheless, strong variation in the Kelvin wave activity is also observed outside of the envelope of prevailing MJO convection, which has not been closely examined in previous studies. For example, over South America and the tropical Atlantic Ocean, while the MJO convection anomalies are weak, the Kelvin wave activity shows strong variation comparable to those within the MJO convection envelope (e.g., in phases 1 and 2). Similar features can be found to the north of the equator over the central Pacific (see phases 3 and 4). One thing we need to consider with caution is that the MJO often excites planetary extratropical Rossby wave trains in both hemispheres during particular MJO phases, and the Kelvin filter will capture these eastward-propagating extratropical Rossby waves falsely outside of the deep tropics. Nevertheless, the latitudinal average that we apply in this study is between 15°S and 15°N, which should reduce this complication to a negligible level. In this study, we will focus on the South America and Atlantic region, although the central Pacific Ocean is also an interesting region to be examined in future studies. To be more specific, the region that we will focus on is 15°S–15°N, 80°W–0° (pink box in phase 1 of Fig. 2). More careful examination reveals that the Kelvin wave activity in this region is enhanced during MJO phases 8, 1, and 2, while it is reduced during MJO phases 4, 5, and 6. In particular, strongest positive (negative) Kelvin wave activity anomaly appears in phase 1 (5). In addition, almost all the points within the shaded area are significant at the 99% confidence level based on a one-tailed Student's *t* test; thus, no significance contour is added to this figure.

Figure 2 clearly shows the enhancement or suppression of the Kelvin wave activity over the South America and tropical Atlantic region with respect to particular MJO phases. Nevertheless, wave activity in terms of variance is a quantity summarizing the behavior of an ensemble of waves for days in a given phase and does not provide detailed information such as the typical wave amplitude and zonal wavenumber (or wavelength) of the CCKWs or the frequency of occurrence of CCKWs with specific wave amplitude and wavenumber in this phase. The wave amplitude is the direct indicator of the wave strength, while zonal wavenumber (wavelength) is an essential part of the wave structure. Going beyond a simple variance measure, such features are important to understand as they characterize the higher frequency (i.e., weather) aspects of the MJO's modulation. Thus, in next subsections, we will examine how the MJO modulates the wave strength and the horizontal and vertical wave structures of the individual CCKWs.

b. *MJO modulation of the wave amplitude and wavenumber of CCKWs*

In this study, a simple method to derive the daily wave amplitude and wavenumber of the CCKW over the South America and tropical Atlantic region is applied. For each

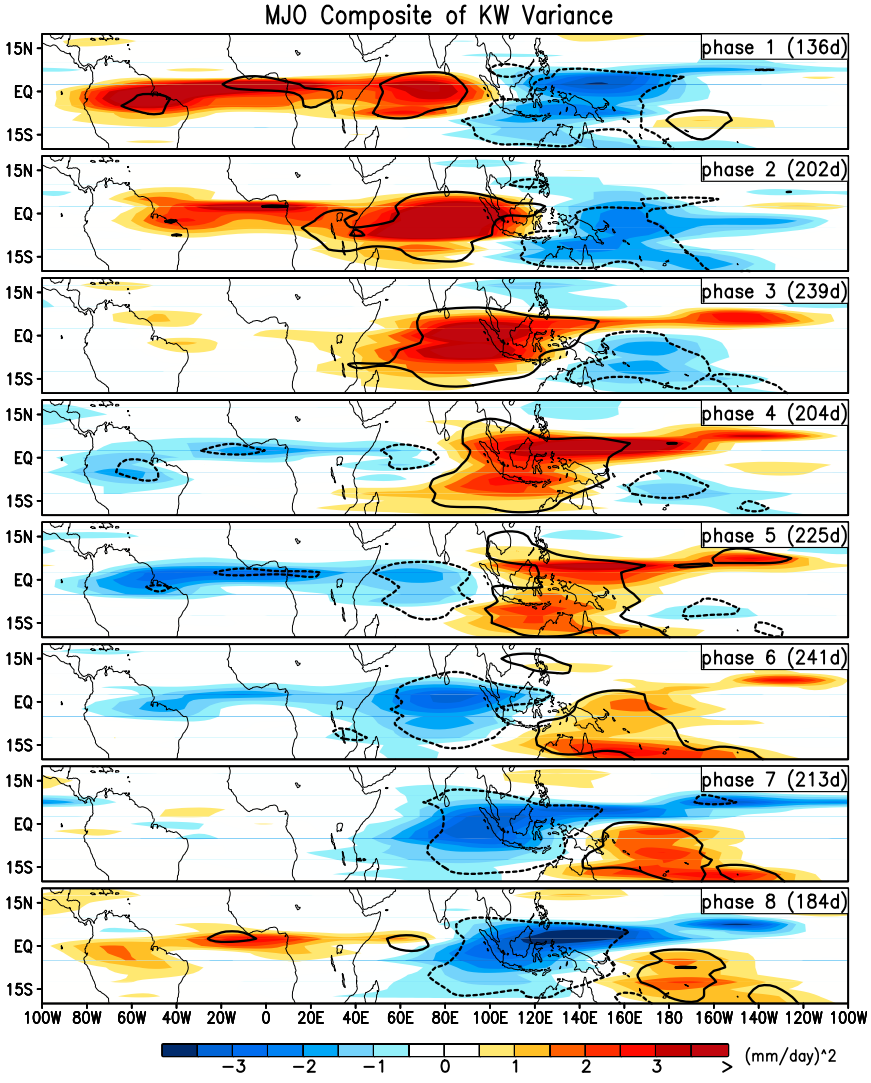

FIG. 2. Eight-phase MJO composite patterns of the 30–96-day-filtered variance of the Kelvin-filtered TRMM rainfall (shaded; $mm^2\,day^{-2}$) during the 1998–2012 winter seasons. Only strong MJO days are used. Superimposed are the +0.81 (black solid) and −0.81 mm day^{-1} (black dashed) contours of the composite MJO anomalies; 0.81 mm day^{-1} corresponds to half of the mean standard deviation averaged over the entire tropics (15°S–15°N, 0°–360°E) during the 1998–2012 winter seasons. Pink box shows the specific region of the focus of this paper.

day, the Kelvin-filtered anomalies are averaged in the 15°S–15°N latitudinal band for all points from 80°W to 0°. The wave amplitude is then determined by averaging the absolute values of the resulting anomalies over all these points. The zonal wavenumber is determined by the number of zero crossings of the resulting anomalies. For example, one zero crossing between 80°W and 0° implies a half wavenumber over this region, and two zero crossings correspond to one wavenumber, and so on. Even though this is a rather crude way to quantify the wave amplitude or wavenumber of the CCKW, as will be seen next, our main focus is on the variation of the CCKWs characteristics from one MJO phase to another instead of CCKWs details on any particular day, and hence a simple while consistent way to estimate the wavenumber or wave amplitude is not expected to introduce significant systematic biases to our results.

The mean wave amplitude and wavenumber for the eight MJO phases are then calculated by compositing the daily wave amplitude and wavenumber during the 1998–2012 winters and are shown as the red and blue curves in Fig. 3. The MJO cycle of the mean Kelvin wave activity anomalies (average of the variance anomalies within the pink box in Fig. 2) is also shown as the black

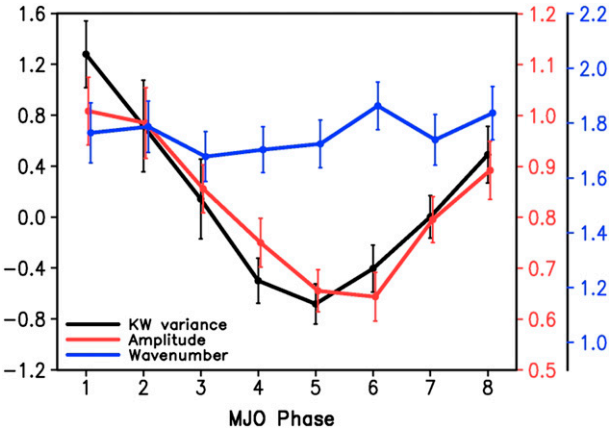

FIG. 3. Eight-phase cycle of the 30–96-day-filtered CCKW variance averaged over 15°S–15°N, 80°W–0° (anomalies averaged over pink box region in Fig. 2; black; $mm^2\ day^{-2}$), the mean Kelvin wave amplitude (red; $mm\ day^{-1}$), and mean wavenumber (blue; unitless) over the same region during the 1998–2012 winter seasons. The error bars denote the 99% confidence level of the means based on a one-tailed Student's *t* test.

curve. We can see that the mean wave amplitude of the CCKWs shows a cycle closely following that of the Kelvin wave variance. As to the mean CCKW wavenumber, it does not show much variation among different MJO phases. Furthermore, the uncertainties in the mean wave activity indicated by the error bars suggest that the systematic variation in the mean wave activity is quite robust and statistically distinguishable among the different MJO phases as the error bars for the mean values exhibit little overlap between opposite phases in the MJO life cycle. This is also true for the mean wave amplitudes, but not for the mean wavenumbers, which have error bars that are largely overlapping among the different MJO phases.

In addition to the mean, the histograms of the wave amplitude and wavenumber of CCKWs for each MJO phase are shown in Fig. 4. For the wave amplitude, the daily values are grouped into 14 bins ranging from 0 to $1.4\ mm\ day^{-1}$ with an interval of $0.1\ mm\ day^{-1}$. Instead of showing the number of days falling within each bin, we show the percentage of number of days relative to the total number of days for a certain MJO phase to facilitate more direct comparison with the climatological distribution as well as comparison between MJO phases since different phases contain different number of strong MJO days (see Fig. 2). The climatological distribution, computed by binning all days regardless of MJO phase, is shown by the black curves in Figs. 4a and 4c. Comparing to the climatology, we find that the wave amplitude exhibits clear shifting toward the stronger amplitude in phases 8, 1, and 2: with a larger (smaller) percentage of days with relatively strong (weaker) amplitudes than climatology (Figs. 4a and 4b). On the contrary, the wave amplitude shifts toward weaker amplitudes for phases 4, 5, and 6. In contrast, Figs. 4c and 4d indicate that there is not much variation in the wavenumber distribution across the eight MJO phases: the histograms for all phases follow the climatological distribution quite closely.

Figures 3 and 4 show that during the MJO phases in which the CCKW activity is increased, the mean Kelvin wave amplitude becomes stronger with the frequency of occurrence of individual Kelvin waves systematically shifts toward the larger amplitudes, and vice versa for the MJO phases with decreased CCKW activity. It is also revealed that the CCKW wavenumber (or wavelength) does not vary much among different MJO phases. These findings provide useful information on how the MJO could influence the weather phenomena closely related to the CCKW.

c. *MJO modulation of the horizontal and vertical structures of CCKWs*

In this subsection, the horizontal and vertical atmospheric structures of the typical CCKWs in each MJO phase are further explored by a linear regression analysis. To construct the reference time series for various dynamical and thermodynamical parameters to be regressed against, an EOF analysis is applied to the equatorially averaged (15°S–15°N) Kelvin-filtered TRMM anomalies on the strong MJO days for each phase, and then the first principal component (PC1) of the EOF analysis is used as the reference time series for that phase. The first and second eigenvectors of each phase are shown in the lower part of each panel in Fig. 5. It can be seen that the first two eigenvectors for any given phase are shifted in longitude by about one-quarter cycle, and the percentages of variance explained by them are very close (the percentage of variance explained by the first EOF mode is shown in Fig. 5). As previous studies have suggested (Wheeler and Hendon 2004), these two leading EOF modes represent the different propagation stages of the same wave. The first and second EOFs together explain more than half of the variance, implying that this wave mode is dominant.

The typical horizontal structures of the CCKWs as indicated by the regressions of the Kelvin-filtered TRMM precipitation and 850-hPa wind anomalies upon PC1 are shown in Fig. 5. In each phase, a wave train with about 1.5–2.0 wavenumbers is exhibited over the South America and tropical Atlantic region, which is consistent with the fact that the median wavenumber is between 1.5 and 2 as shown in Fig. 4c. Difference in the eigenvector amplitude of the CCKWs in different MJO phases is also discerned: the largest eigenvector amplitudes

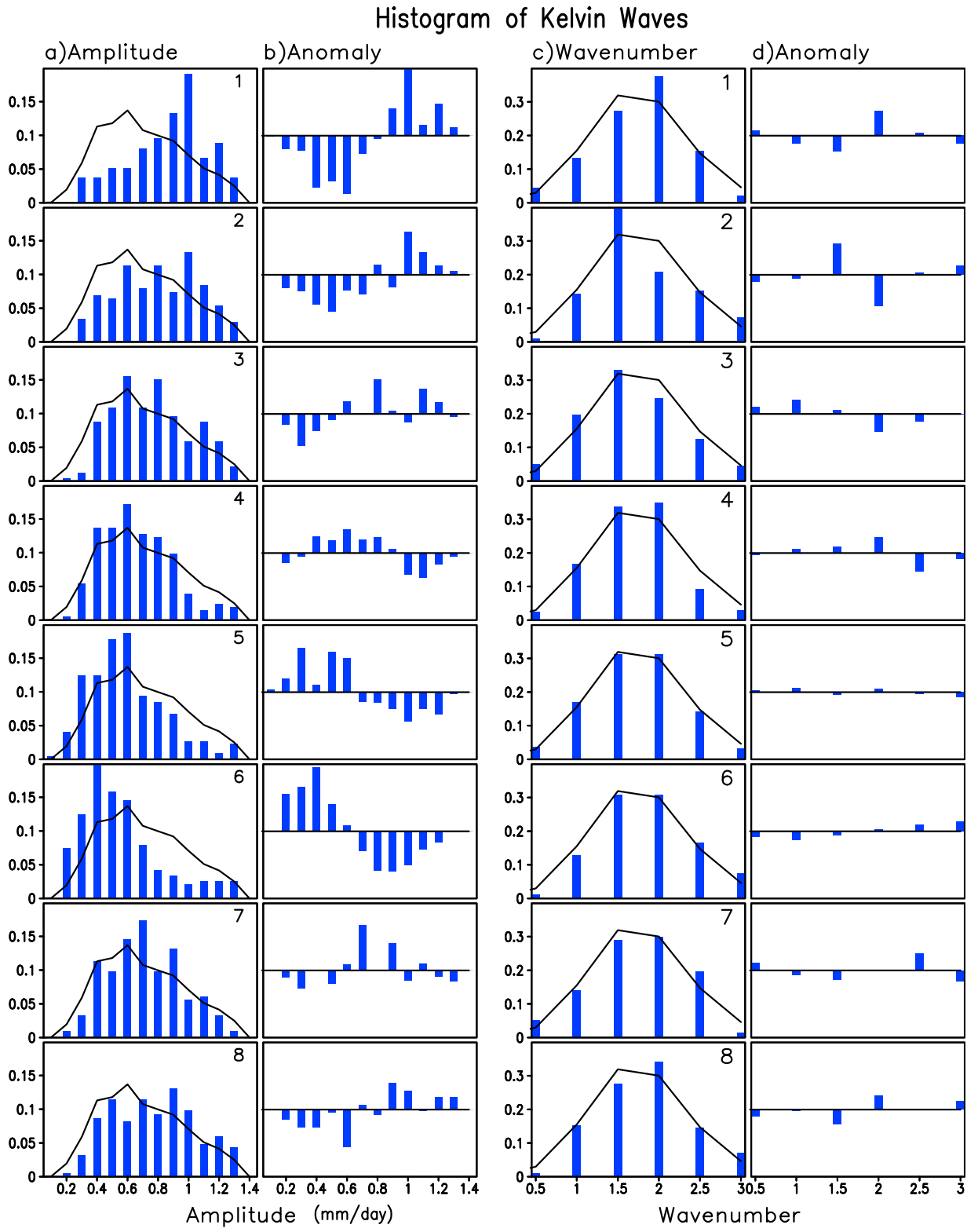

FIG. 4. The histograms of the daily Kelvin wave (a) amplitude (mm day^{-1}) and (c) wavenumber averaged over 15°S–15°N, 80°W–0° during 1998–2012 for the eight MJO phases, with the climatological histograms (black curves) superimposed. The *y* axis is the percentage of total number of days in each wave amplitude or wavenumber bin. Also shown are the anomalies of (b) the amplitude and (d) the wavenumber relative to the climatology.

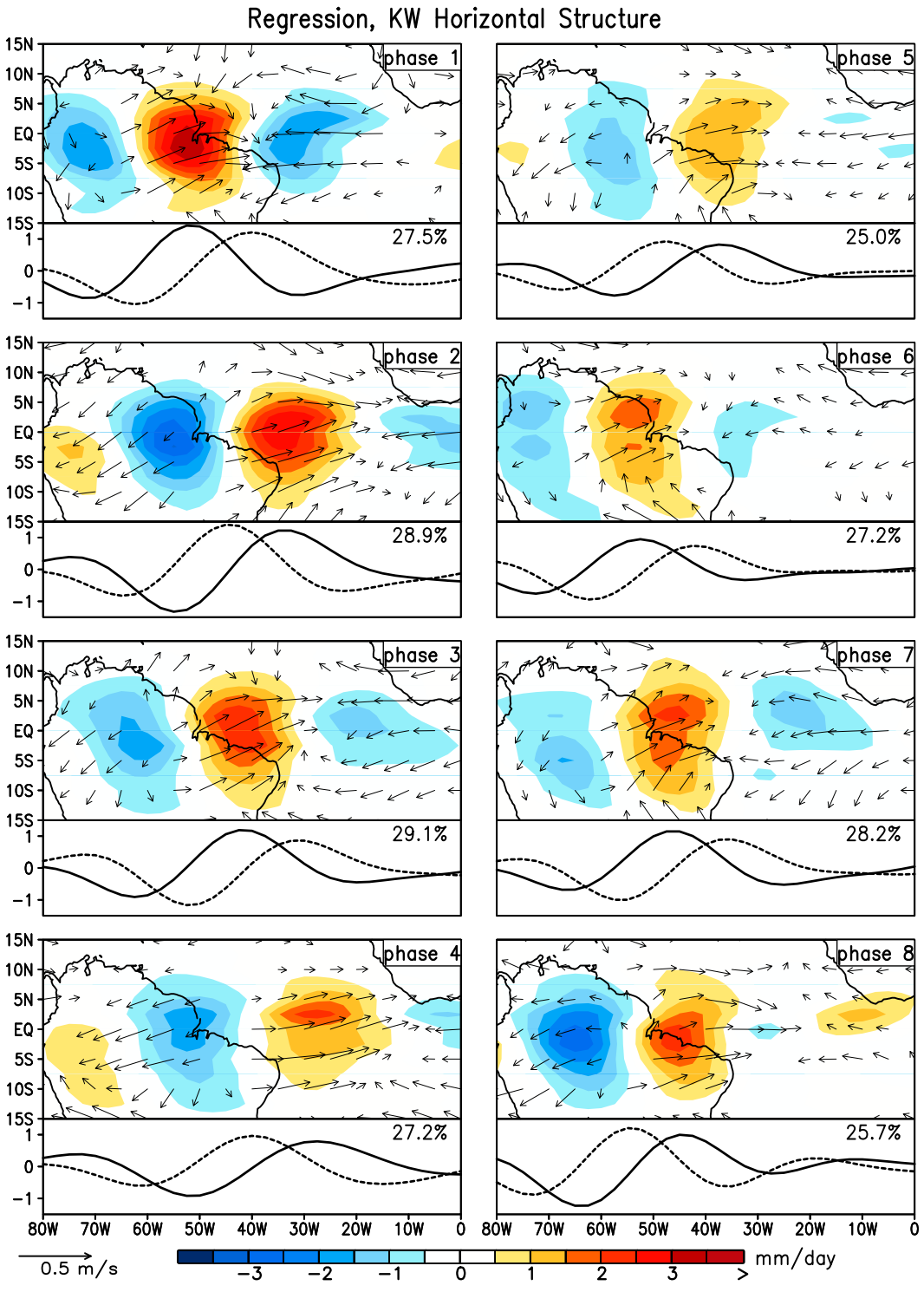

FIG. 5. The typical horizontal Kelvin wave structures in each MJO phase indicated by the regression patterns of Kelvin-filtered TRMM precipitation (shaded; mm day^{-1}) and 850-hPa horizontal wind (arrows; m s^{-1}) anomalies. The reference time series is the first PC of the EOF analysis of the equatorially averaged (15°S–15°N) Kelvin-filtered TRMM anomalies. The first (black solid) and second (black dashed) EOFs are shown under each regression pattern, with the percentage of variance explained by the EOF1 indicated at the upper-right corner.

appear during MJO phases 1 and 2, while the weakest eigenvector amplitudes appear in phases 5 and 6, which is again in agreement with the results for CCKW amplitude shown in section 3. Despite such phase-to-phase variation due to the modulation by the MJO, some common features of the CCKWs are also noted. For example, the low-level convergence appears about 15° east of the positive convection center; meanwhile, the low-level divergence is also located slightly eastward of the negative convection center. These features are consistent with what has been described in previous studies (Straub and Kiladis 2003b).

Keep in mind that the signs of the regression patterns in Fig. 5 are arbitrary since the reference time series is a PC from the EOF analysis; that is, it does not make any difference if we multiply the regression pattern by -1. Also, the regression patterns for the eight MJO phases should never be interpreted as the evolutionary patterns of the same wave in consecutive phases since reference time series are obtained independently for each MJO phase. Instead, these regression patterns should be regarded as the most frequently occurring spatial pattern for each phase, or in other words, the ''typical'' wave pattern, as it is regressed onto PC1 of the EOF analysis. It is appropriate to perform the regression in this way since our focus is on the variation of the CCKWs in different MJO phases rather than on the evolution of individual CCKWs.

Coherent vertical structures of the CCKWs are shown by the longitude–height regression of the Kelvin-filtered zonal wind, specific humidity, and temperature anomalies (averaged between 15°S and 15°N) upon the PC1 of Kelvin-filtered rainfall for each MJO phase (Fig. 6). Again, there is not expected to be an evolutionary relation between the CCKWs in one MJO phase to the next. In Fig. 6a, the CCKWs exhibit a baroclinic mode structure with the wind anomalies tilted westward from the lower to the upper troposphere at around 250 hPa, and then tilted eastward from the upper troposphere to the lower stratosphere. The westerly vertical wind shear to the east of the Kelvin wave active convection as well as the easterly vertical wind shear to its west has been found to be one of the factors important to the Atlantic tropical cyclogenesis by modifying the background wind shear (Ventrice et al. 2012b). The westward tilt with altitude associated with the CCKWs is also evident in the specific humidity field, with the positive humidity anomalies roughly aligned with the convergence anomalies in the tropospheric wind anomaly field. The specific humidity anomalies are mainly confined to the lower to middle atmosphere. In contrast to the wind and humidity fields, the temperature anomalies are mainly characterized by a second-baroclinic-mode structure, with warm over cold anomalies in the region of active convection, and cold over warm anomalies to the east of the active convection region, with pronounced variation found in the middle troposphere as well as in the boundary layer. These features of the CCKW vertical structure are largely consistent with previous results based on analysis over the Pacific region (e.g., Straub and Kiladis 2003b). The modulation of the vertically regressed CCKW patterns by the MJO is again mainly characterized by the variation in the wave amplitude, with much stronger amplitude in phases 1 and 2 than that in phases 5 and 6, which is similar to what we have found in the horizontal patterns. In addition to the amplitude variation, the MJO seems to exert some modulation on the vertical tilting. For example, the westward tilt of the zonal wind anomalies appears to be considerably stronger in phases 1 and 2 than that in phases 6 and 7; the variation of the tilt in the humidity field is not as evident as that in the wind field, but still noticeable (see the black dashed lines in Figs. 6a and 6b). The degree of westward tilt is roughly estimated by the longitude difference between the positive maximum point at 850 hPa and that at 500 hPa (the number at the lower-right corner of each panel in Figs. 6a and 6b). It is also noted that the stronger (weaker) westward tilt appears to be roughly associated with the stronger (weaker) wave amplitude although the relation is not very robust.

4. Physical mechanisms

In section 3, we have found that the MJO exerts clear modulation on the CCKW activity over South America and the tropical Atlantic Ocean. The modulation is mainly characterized by increased CCKW amplitude in certain MJO phases (most evident in phase 1) and suppressed wave amplitude in other phases (most evident in phase 5), with secondary impacts on wave structure. In this section, we will explore some possible physical processes through which the MJO might modulate the CCKW activity over this region.

Previous studies have indicated that the vertical shear of the large-scale environmental flow has been found to modulate the structure and instability properties of convectively coupled equatorial waves. For example, a theoretical study by Zhang and Geller (1994) suggested that equatorial Kelvin waves are selectively favored by basic flows with easterly vertical wind shear. Specifically, under wave–conditional instability of the second kind (CISK) theory, they illustrated that the growth of waves and the generation of potential energy require unstable waves to tilt with height in a direction opposite to that of their propagation, while extraction of mean-flow potential energy requires the wave tilt to be against the vertical shear; thus, easterly vertical shear promotes CISK for

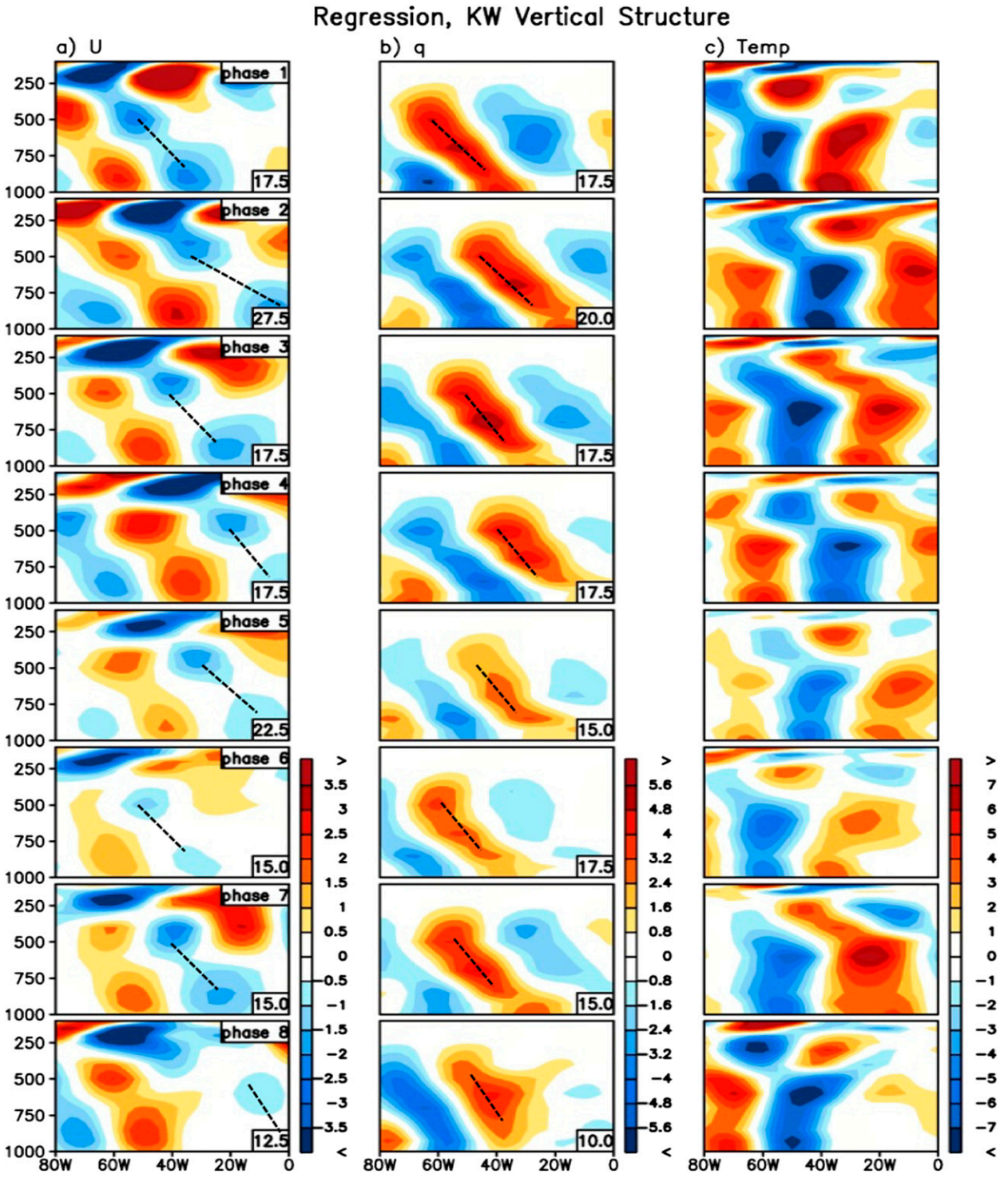

FIG. 6. The typical vertical Kelvin wave structures in each MJO phase indicated by the regression patterns of Kelvin-filtered (a) zonal wind (10^{-1} m s^{-1}), (b) specific humidity (10^{-4} kg kg^{-1}), and (c) temperature anomalies (10^{-2} K). The reference time series is as in Fig. 5. Black dashed line in (a),(b) illustrates the westward tilt of the Kelvin wave with the longitude difference between the positive maxima at 850 and 500 hPa along this tilt indicated at lower-right corner.

eastward-propagating Kelvin waves, while westerly vertical shear suppresses them. Based on a cloud-resolving model study, Wu and LeMone (1999) showed that the envelope of the precipitating clouds within a convectively active phase of the MJO changes from westward moving to eastward moving when the surface confined (below 2 km) westerlies deepen to 5 km while both are topped by easterlies at the upper level. Numerical experiments by Li (2006) also revealed that the basic-state vertical shear may affect the growth rate and propagation character of the synoptic-scale wave train. More recently, a series of studies based on a so-called ''multicloud'' model have further illustrated that the vertical shear of planetary-scale environmental flow of the MJO can regulate the behaviors of the convectively coupled equatorial waves by favoring either eastward- or westward-propagating waves, but the relation between the enhancement of the convectively coupled equatorial waves and various background wind shear is rather complex (Han and Khouider 2010; Majda and Stechmann 2009; Khouider et al. 2012). For example, their model results (Han and Khouider 2010) did suggest that the increased easterly wind shear leads to enhanced Kelvin wave instability; however, it is also true for the westerly wind shear situation.

The importance of the tropospheric moisture in regulating tropical convection is more self-evident, as it can be easily understood that the air tends to be humid when and where there is sustained deep convective rainfall and vice versa. A large number of studies have addressed the role of low- to midtroposphere moisture in helping initiate tropical deep convection (e.g., Numaguti et al. 1995; Ushiyama et al. 1995; Brown and Zhang 1997; Sherwood 1999; Sherwood and Wahrlich 1999; Sobel et al. 2004; Bretherton et al. 2004). Moreover, increasing evidence shows that lower- to middle-tropospheric moisture also plays a key role in regulating convection associated with the synoptic-scale convectively coupled waves and the MJO (e.g., Chao 1987; Kikuchi and Takayabu 2004; Kiladis et al. 2005; Khouider and Majda 2008; Thayer-Calder and Randall 2009; Zhu et al. 2009).

Thus, in this work, we examine the vertical wind shear and the lower- to middle-troposphere moisture anomalies as chief elements of the large-scale dynamical and thermodynamical influences of the MJO and their systematic relationships to variations in CCKW activity. The composites of the MJO-filtered vertical zonal wind shear and specific humidity anomalies for the eight MJO phases are shown in Figs. 7b and 7c, respectively. The MJO composite of the 30–96-day-filtered CCKW activity in terms of TRMM precipitation is also shown (Fig. 7a) for reference. The vertical zonal wind shear is computed as the zonal wind difference between 700 and 200 hPa (700 minus 200 hPa), which captures the strongest lower- to upper-troposphere zonal wind shear (see Fig. 9a below). Note that conventionally the wind shear is defined as the upper-level wind minus the lower-level wind. The negative of this convention used here is used to facilitate the direct comparison to the CCKW variation (see Figs. 7a and 7b). The composite specific humidity anomalies shown in Fig. 7c are integrated from 850 to 500 hPa to represent lower- to middle-troposphere water vapor content. Note that our results are not qualitatively sensitive to the choice of the levels used to compute the wind shear or the integral of the specific humidity if varied within a reasonable range. Furthermore, as we mentioned in section 3a, almost all the points within the shaded area in the composite map of the CCKW activity (Fig. 7a) are significant at a 99% confidence level based on a one-tailed Student's t test. The shaded area in the MJO composite maps for all MJO-filtered variables (Figs. 7b,c, 8, and 9) are significant at an even higher confidence level, which is not surprising since the MJO filtering has extracted the signals associated with the MJO, and the composite is based on the RMM index that is supposed to distinguish the eight MJO phases by design. Thus, no additional contours regarding the significance level of the composite means are added in all these composite maps (Figs. 7–9).

Figure 7b shows the composites of the MJO-filtered vertical zonal wind shear anomalies. Pronounced anomalous easterly wind shear exists in the entire region of interest in MJO phases 1, 2, and 3, while pronounced anomalous westerly wind shears are found in phases 5, 6, and 7. In particular, the largest easterly and westerly wind shear anomalies are found in phase 2 and phase 6, respectively. Rather weak wind shear anomalies are noted during phases 4 and 8.

Figure 7c shows the composites of the MJO-filtered specific humidity anomalies integrated in the lower to middle troposphere. Variations of the specific humidity over the eight MJO phases are also very evident: negative humidity anomalies dominate from phases 2 to 5, while positive humidity anomalies dominate in phases 6, 7, 8, and 1. The strongest negative and positive anomalies are found in phase 3 and phase 8, respectively. Compared to the vertical wind shear, the specific humidity anomalies exhibit more geographical variation and generally exhibit a horizontal tilt from the southwest to the northeast over the region.

Recall that the largest enhancement of the CCKW activity occurs in phase 1, and the largest suppression is in phase 5 (Fig. 7a). Thus, neither the vertical wind shear nor the lower- to middle-tropospheric water vapor content exhibits an identical evolution, in terms of both sign and magnitude over the eight phases, with the CCKW activity over the eight-phase MJO cycle. However, when

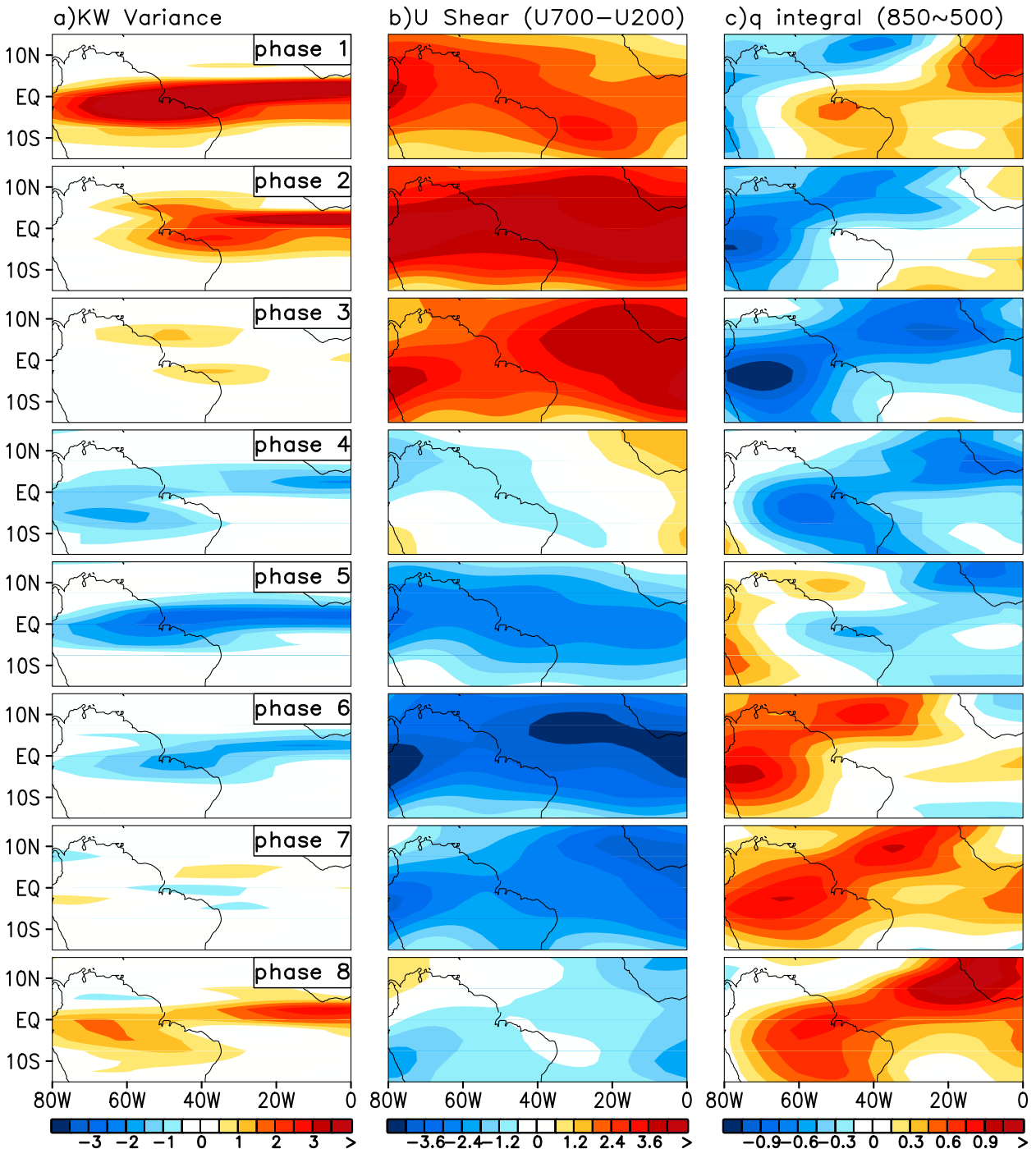

FIG. 7. Eight-phase MJO composite patterns of (a) the 30–96-day-filtered CCKW variance ($mm^2\ day^{-2}$), and the MJO-filtered (b) vertical shear of zonal wind between 700 and 200 hPa ($m\ s^{-1}$) and (c) specific humidity integrated from 850 to 500 hPa ($kg\ kg^{-1}$).

considered together, variations in these two parameters appear to be able to explain the evolution of the CCKW activity during the MJO cycle. In phase 1, both the easterly wind shear and the overall positive moisture anomalies favor the enhancement of CCKW activity. In phase 2, the easterly wind shear is even stronger than that in phase 1; however, the anomalous water vapor content becomes negative. The combined effect thus leads to a weaker enhancement of the CCKW activity compared to that in phase 1. The water vapor content is further reduced in phase 3, and meanwhile the easterly shear also becomes weaker, which results in a very weak

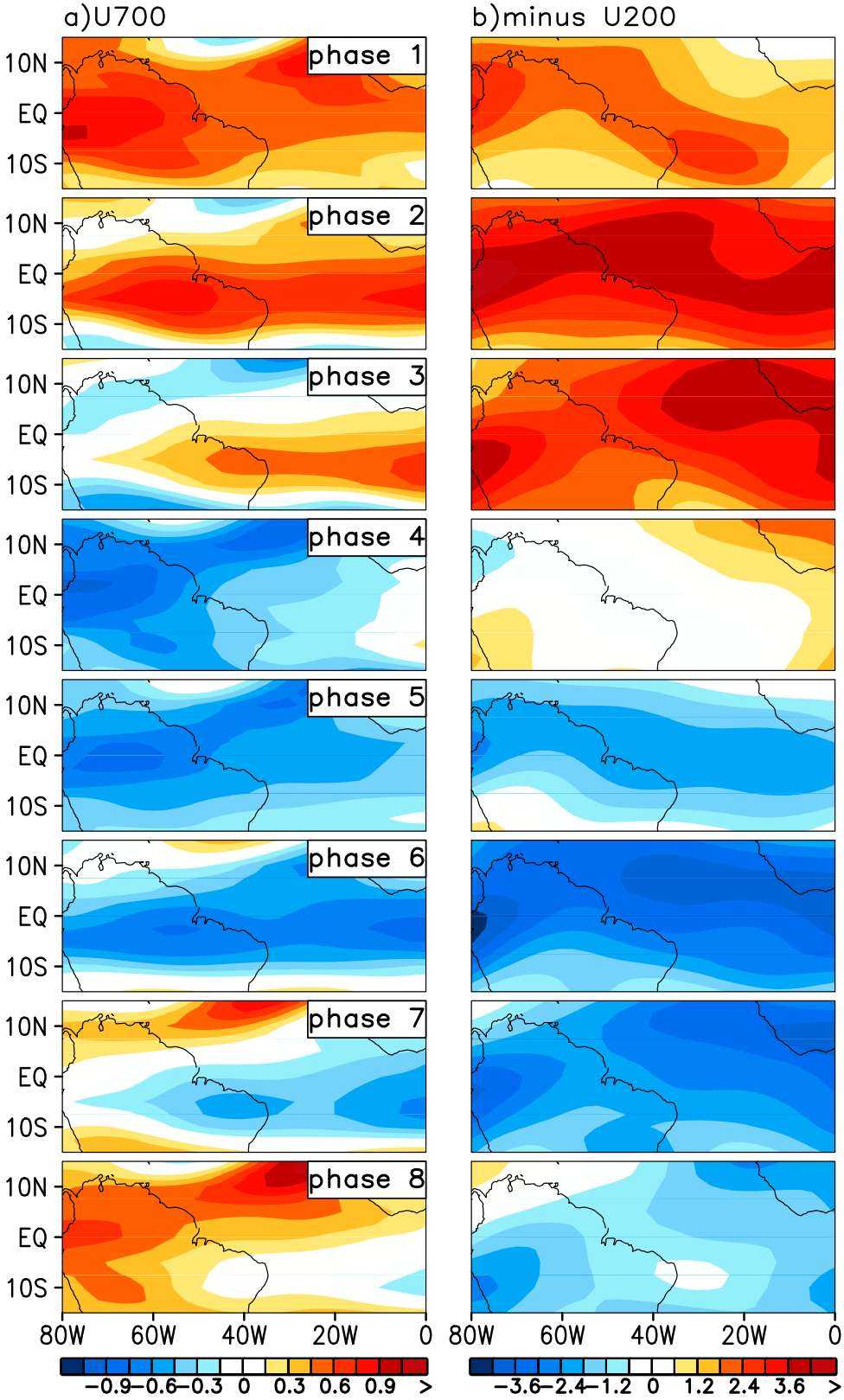

FIG. 8. Composite anomalous patterns of the MJO-filtered (a) 700-hPa and (b) reversed 200-hPa zonal wind ($m\,s^{-1}$) during the eight MJO phases.

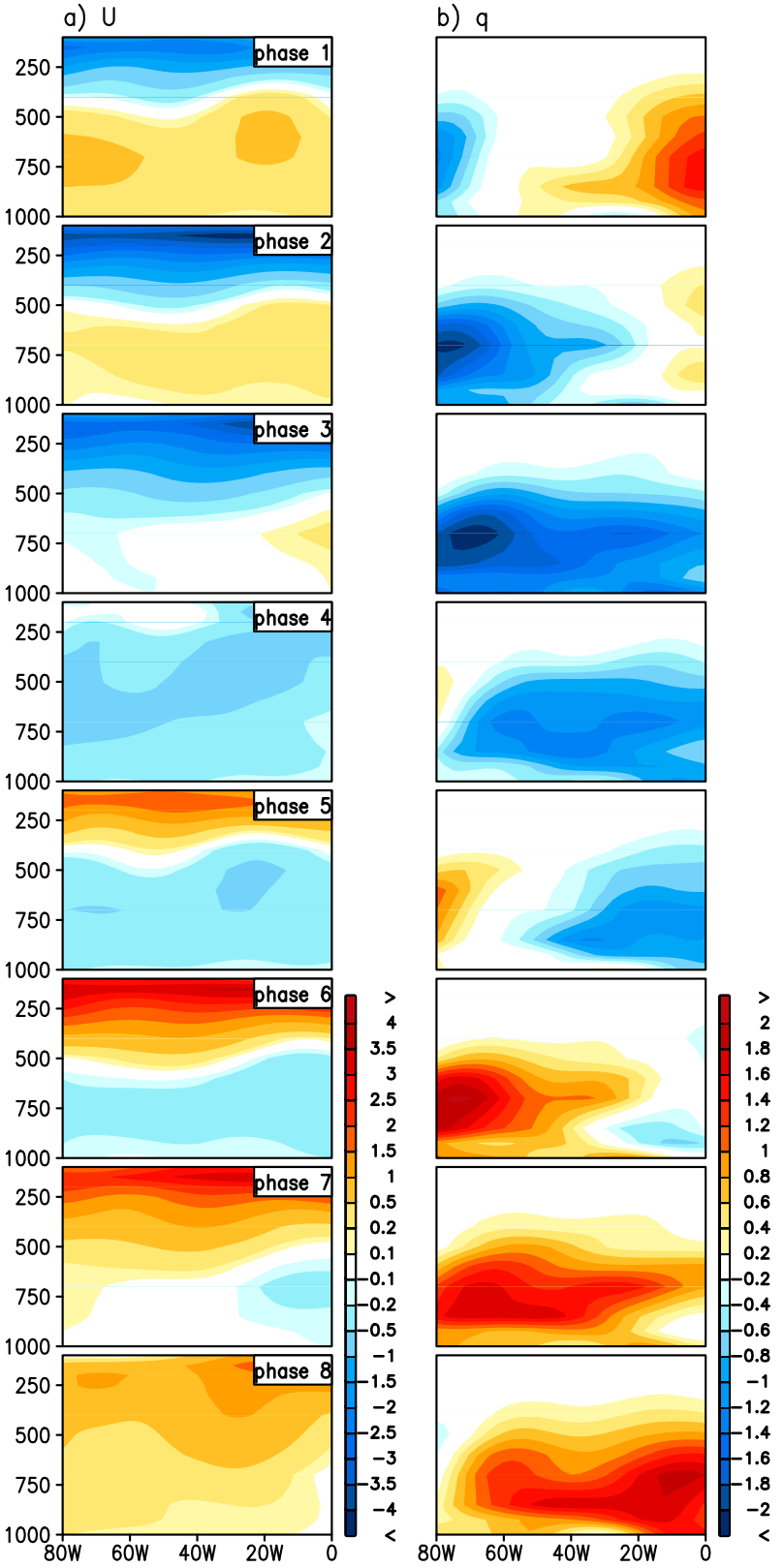

FIG. 9. Longitude–pressure profiles of the composite MJO-filtered (a) zonal wind ($m\,s^{-1}$) and (b) specific humidity ($10^{-4}\,kg\,kg^{-1}$) anomalies averaged between 15°S and 15°N.

enhancement in the CCKW activity. In phase 4, the wind shear changes from strong easterly to weak westerly, and the water vapor anomalies are still quite negative; thus, both factors tend to suppress the CCKW activity. Phases 5–8 largely mirror phases 1–4. For example, despite the strong moist anomaly in phase 7, the wind shear anomalies are strong negative (westerly shear anomalies) and thus strongly suppress the CCKW activity. Note that owing to its ''trapped'' nature, the CCKW activity is narrowly confined to near the equator although the wind shear and moisture anomalies occupy a much broader region meridionally. These results suggest that vertical wind shear and lower- to middle-tropospheric water vapor content could be two competing factors/influences in regulating CCKW activity; the variation in CCKW activity during the MJO cycle may only be explained by combing effects from both of these two effects. More rigorous support for this hypothesis, however, will need support from future studies—for example, by conducting idealized model experiments. For example, a recent idealized model study by Khouider et al. (2012) suggested the same importance of these two effects in enhancing or weakening the synoptic and mesoscale convective instability.

The vertical zonal wind shear consists of the wind difference between the lower and upper troposphere. A previous study by Han and Khouider (2010) also suggested that it is not only the vertical shear but also the variation in the individual wind in either the lower or the upper level that can impact the growth rate of the Kelvin waves. Thus, we further illustrate the eight-phase composites of the MJO-filtered zonal wind anomalies at 700 and 200 hPa in Figs. 8a and 8b, respectively. Note that the sign of 200-hPa u wind is reversed to be consistent with the wind shear anomaly pattern in Fig. 7b. First, it is seen that the MJO composite patterns of the 200-hPa u-wind anomalies are very similar to those of the vertical wind shear also with a comparable magnitude, which indicates that the vertical wind shear anomalies are largely associated with the upper wind anomalies. The magnitude of 700-hPa wind anomalies is only about 1/5 of that at 200-hPa wind anomalies, and overall they are largely opposite to the 200-hPa wind. One thing interesting about the composite 700-hPa wind anomalies is that its MJO cycle leads that of the reversed 200-hPa wind by approximately one phase and thus is concurrent with the MJO cycle of the CCKW activity anomalies. This better consistency might suggest some critical role that the low-level circulation plays in exciting the Kelvin waves. However, more detailed studies are needed in order to draw any solid conclusions on this point. Furthermore, the variation in the westward tilt of the CCKWs found in section 3c might be related to the variation in the low- and upper-level winds. For example, the anomalous low-level westerlies and upper-level easterlies in phases 1, 2, and 3 might be related to the stronger westward tilt in these phases. On the contrary, the anomalous low-level easterlies and upper-level westerlies might contribute to the weaker westward tilt in phases 6 and 7.

Furthermore, the vertical structures of the MJO-filtered zonal wind and specific humidity anomalies from 1000 to 100 hPa are shown for the eight MJO phases (Fig. 9). The anomalies are averaged between 15°S and 15°N. It is shown that the zonal wind anomalies associated with the MJO are generally in opposite direction below and above about 500 hPa except for phases 4 and 8 in which the upper-level wind anomalies are remarkably weaker compared to the other phases and have the same direction with the low-level wind anomalies. The amplitude of the upper-level wind anomalies dominate the low-level wind anomalies and are strongest in phases 2 and 6. As previously mentioned, a better phase consistency between the low-level wind anomalies and the CCKW activity anomalies is again noted. The specific humidity anomalies associated with the MJO are found to be confined within the lower to middle troposphere, with maximum variation occurring at around 800–700 hPa. It is noticed that there is much smaller variation near the surface and in the boundary layer, which is consistent with the results of Holloway and Neelin (2009) that radiosonde moisture profiles conditionally averaged on precipitation show a strong association between rainfall and moisture variability in the free troposphere peaking at around 800 hPa and little boundary layer variability.

Finally, the above results on the relation between the MJO composites of the 30–96-day-filtered CCKW activity anomalies and the MJO-filtered vertical wind shear and lower- to middle-tropospheric moisture content anomalies are summarized in Fig. 10a, in which the anomalies in each phase are averaged over the entire domain (15°S–15°N, 80°W–0°). The quantities in Fig. 10 are plotted in a way that their scales in the y direction are roughly proportional to their ranges of their variation in magnitude. Although the above scaling should not be overinterpreted as to give a quantitative relation between the variation in wind shear/water vapor and the variation in the CCKW activity, it clearly reveals that the competition between the wind shear and lower- to middle-tropospheric water vapor content produces the observed MJO cycle of the CCKW activity. The vertical wind shear has a variation lagging about one phase that in the CCKW activity, while the water vapor content shows a variation leading about two phases ahead of it. Here, we suggest that the cancellation between the two factors in phases 2, 3, 6, 7, and 8 as well as the reinforcement between them in phases 1, 4, and 5 overall produce the MJO cycle of the

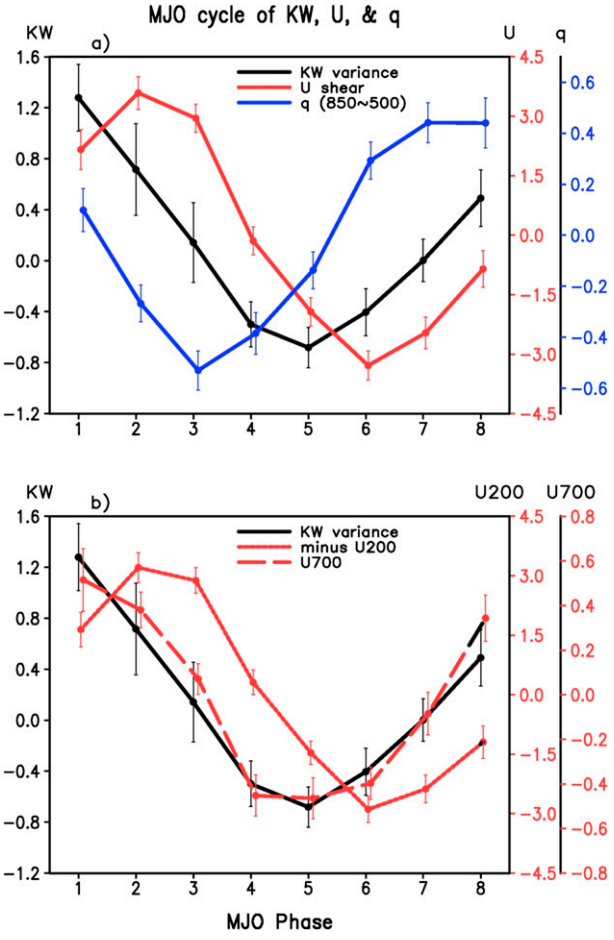

FIG. 10. (a) The MJO cycle of the 30–96-day-filtered CCKW variance (black; $mm^2\,day^{-2}$), the MJO-filtered vertical shear of zonal wind between 700 and 200 hPa (red; $m\,s^{-1}$), and specific humidity integrated from 850 to 500 hPa (blue; $kg\,kg^{-1}$). (b) As in (a), but for the MJO-filtered 700-hPa zonal wind (red long dashed; $m\,s^{-1}$) and reversed 200-hPa zonal wind (red short dashed; $m\,s^{-1}$). The error bars denote the 99% confidence level of the means based on a one-tailed Student's *t* test.

CCKW anomalies. It is further noted that the cycle of the low-level wind anomalies follows the MJO cycle of the CCKW anomalies very well, while the reversed upper-level wind anomalies exhibit a lag of one phase relative to the CCKW anomalies (Fig. 10b).

One point that we should be careful about here is that the phase lag of the wind shear with respect to the CCKW activity does not mean that the change in CCKW activity results in the wind shear change one phase later. Similarly, it is not the case that the water vapor leading CCKW activity implying water vapor anomalies are the entire cause the change in CCKW anomalies. Instead, as we are suggesting that it is the combination of, and phase relationships between, the two physical factors relative to the CCKW activity that produces the observed MJO cycle of the CCKW activity.

Another thing about the CCKW activity in phase 1 is that it exhibits a particularly strong enhancement, and the enhancement in the easterly wind shear and water vapor content together seems not to be strong enough to explain the magnitude of the CCKW enhancement if we compare the relative scaling of the CCKW activity, wind shear, and water vapor content in phase 1 with that in other phases. One possible reason for this magnitude discrepancy is that there could be a nonlinear effect between the positive wind shear and water vapor anomalies. Another possible reason is that there may exist other physical mechanisms: for example, horizontal wind shear/vorticity, lower-level moisture convergence, convective momentum transport, and even possible influence by the strong Atlantic aerosols. We have looked at some of the above mechanisms, but no solid conclusions are yet reached. More thorough examinations of the physical mechanisms responsible for the variation in the Kelvin wave activity are of future interest.

5. Conclusions and discussion

The CCKW activity over the South America and tropical Atlantic region exhibits strong variation with comparable magnitude to that over the Pacific region on both climatological and intraseasonal time scales. In this work, modulation of the CCKW activity over this region by the MJO has been investigated. The CCKW activity is found to be enhanced during MJO phases 8, 1, and 2 (most evident in phase 1) and suppressed during MJO phases 4, 5, and 6 (most evident in phase 5). Analysis of wave amplitude and wavenumber of individual CCKWs during different MJO phases reveals that the enhancement (suppression) of the CCKW activity is primarily characterized by the increased (decreased) CCKW amplitude, with the amplitude modulation evident throughout the troposphere and even into the stratosphere in wind and temperature fields. Modest MJO modulation on the vertical structure (e.g., westward tilt of the CCKWs) is also found, with stronger (weaker) westward tilt tending to accompany the increased (decreased) CCKW amplitude. The zonal wavenumber of CCKWs does not show much variation across the MJO phases.

Plausible physical mechanisms responsible for the modulation of CCKWs by the MJO are also explored. Our results indicate that CCKW variation can be largely explained by considering contributions from two factors: namely, the vertical zonal wind shear and the lower- to middle-troposphere moisture content. For example, in MJO phase 1, both the easterly vertical wind shear and the lower- to midtropospheric positive moisture anomalies tend to amplify the CCKW activity, thus resulting in the strongest CCKW activity in this phase; in phase 2, the easterly wind shear associated with the MJO is even

stronger, while the anomalous moisture content becomes negative overall. These combined effects thus lead to weaker enhancement of the CCKW activity compared to that in MJO phase 1, and similarly for MJO phase 3. In phase 4, the easterly wind shear changes to the westerly shear, which suppresses the CCKW and, at the same time, the moisture content is negative overall, leading to suppressed CCKW activity, and so on for the other phases. The cancellation of these physical processes in phases 2, 3, 6, 7, and 8 as well as the reinforcement from them in phases 1, 4, and 5 overall produces the observed MJO cycle of the CCKW activity anomalies. The variation of vertical wind shear may also be responsible for the modification in the westward tilting of the CCKW during different MJO phases. Additional investigation, however, is needed to further elaborate this point. Additionally, the enhancement of CCKW activity in phase 1 is so strong that the enhancement in both the easterly wind shear and water vapor content seems not to be enough to explain it, which suggests there may exist other physical mechanisms regulating the variation of the CCKW activity, which will be of interest in the future. Moreover, our discussions on the relationship between the vertical wind shear and lower- to middle-tropospheric moisture content and the CCKW activity are mainly based on the correlation analyses. These hypotheses will need to be further substantiated through theoretical and numerical approaches.

Our results indicate that in certain MJO phases, the large-scale dynamical and thermodynamical conditions associated with the MJO favor or suppress the growth of the CCKWs over the South America and tropical Atlantic region. Given the close relationship between the CCKWs and the local as well as downstream weather, the findings in this study have broader implications on extended-range predictability of weather/climate variability. Given predictability of the MJO out to about 4 weeks (e.g., Waliser 2011) and continuous improvement of the predictive skill for the MJO in current general circulation models (GCMs; e.g., Vitart and Molteni 2010; Rashid et al. 2011), the results in this study indicate how such predictability might be leveraged for forecasting CCKW activity and related tropical waves and synoptic disturbances over this region.

In addition, our results suggest possible linkage between the upstream CCKWs and the initiation of the MJO in the tropical western Indian Ocean: enhanced CCKW variance extending from the South America to the Indian Ocean is first evident in phase 8 and gets most pronounced in phase 1; given that phases 8 and 1 roughly correspond to the initiation stage of the MJO cycle composited through RMM indices, our results suggest that the CCKWs excited in upstream as well as their propagating into the western equatorial Indian Ocean could play potentially important roles in the initiation of the MJO. This hypothesis is also implied by Ventrice et al. (2012b) in their Fig. 10. Thus, a better understanding of the CCKW as illustrated in this study could further lead to improved MJO forecast skill.

Acknowledgments. This work was supported by the Marine Meteorology Program of the Office of Naval Research under Project ONRBAA12-001, NSF Climate and Large-Scale Dynamics Program under Awards AGS-1221013 and AGS-1228302, and NOAA MAPP Program under Award NA12OAR4310075. The contribution from D. Waliser to this study was performed on behalf of the Joint Institute for Regional Earth Science and Engineering (JIFRESSE) at the University of California, Los Angeles, and the Jet Propulsion Laboratory, California Institute of Technology, under a contract with the National Aeronautics and Space Administration.

REFERENCES

Bretherton, C. S., M. E. Peters, and L. E. Back, 2004: Relationships between water vapor path and precipitation over the tropical oceans. *J. Climate,* **17,** 1517–1528.

Brown, R. G., and C. Zhang, 1997: Variability of midtropospheric moisture and its effect on cloud-top height distribution during TOGA COARE. *J. Atmos. Sci.,* **54,** 2760–2774.

Chang, C.-P., and H. Lim, 1988: Kelvin wave-CISK: A possible mechanism for the 30–50 day oscillations. *J. Atmos. Sci.,* **45,** 1709–1720.

Chao, W. C., 1987: On the origin of the tropical intraseasonal oscillation. *J. Atmos. Sci.,* **44,** 1940–1949.

Cho, H.-R., K. Fraedrich, and J. T. Wang, 1994: Cloud clusters, Kelvin wave–CISK, and the Madden–Julian oscillations in the equatorial troposphere. *J. Atmos. Sci.,* **51,** 68–76.

Dee, D. P., and Coauthors, 2011: The ERA-Interim reanalysis: Configuration and performance of the data assimilation system. *Quart. J. Roy. Meteor. Soc.,* **137,** 553–597, doi:10.1002/qj.828.

Dunkerton, T. J., and F. X. Crum, 1995: Eastward propagating ~2- to 15-day equatorial convection and its relation to the tropical intraseasonal oscillation. *J. Geophys. Res.,* **100** (D12), 25 781–25 790.

Emanuel, K. A., 1987: An air-sea interaction model of intraseasonal oscillations in the tropics. *J. Atmos. Sci.,* **44,** 2324–2340.

Han, Y., and B. Khouider, 2010: Convectively coupled waves in a sheared environment. *J. Atmos. Sci.,* **67,** 2913–2942.

Holloway, C. E., and J. D. Neelin, 2009: Moisture vertical structure, column water vapor, and tropical deep convection. *J. Atmos. Sci.,* **66,** 1665–1683.

Huffman, G. J., and Coauthors, 2007: The TRMM Multisatellite Precipitation Analysis (TMPA): Quasi-global, multiyear, combined-sensor precipitation estimates at fine scales. *J. Hydrometeor.,* **8,** 38–55.

Khouider, B., and A. J. Majda, 2008: Equatorial convectively coupled waves in a simple multicloud model. *J. Atmos. Sci.,* **65,** 3376–3397.

——, Y. Han, A. J. Majda, and S. N. Stechmann, 2012: Multiscale waves in an MJO background and convective momentum transport feedback. *J. Atmos. Sci.,* **69,** 915–933.

Kikuchi, K., and Y. N. Takayabu, 2004: The development of organized convection associated with the MJO during TOGA

COARE IOP: Trimodal characteristics. *Geophys. Res. Lett.,* **31,** L10101, doi:10.1029/2004GL019601.

Kiladis, G. N., K. H. Straub, and P. T. Haertel, 2005: Zonal and vertical structure of the Madden–Julian oscillation. *J. Atmos. Sci.,* **62,** 2790–2809.

——, M. C. Wheeler, P. T. Haertel, K. H. Straub, and P. E. Roundy, 2009: Convectively coupled equatorial waves. *Rev. Geophys.,* **47,** RG2003, doi:10.1029/2008RG000266.

Li, T., 2006: Origin of the summertime synoptic-scale wave train in the western North Pacific. *J. Atmos. Sci.,* **63,** 1093–1102.

Liebmann, B., G. N. Kiladis, L. M. V. Carvalho, C. Jones, C. S. Vera, I. Bladé, and D. Allured, 2009: Origin of convectively coupled Kelvin waves over South America. *J. Climate,* **22,** 300–315.

——, ——, D. Allured, C. S. Vera, C. Jones, L. M. V. Carvalho, I. Bladé, and P. L. M. Gonzáles, 2011: Mechanisms associated with large daily rainfall events in northeast Brazil. *J. Climate,* **24,** 376–396.

Madden, R., and P. Julian, 1971: Detection of a 40–50 day oscillation in the zonal wind in the tropical Pacific. *J. Atmos. Sci.,* **28,** 702–708.

——, and ——, 1972: Description of global-scale circulation cells in the tropics with a 40–50 day period. *J. Atmos. Sci.,* **29,** 1109–1123.

Majda, A. J., and S. N. Stechmann, 2009: The skeleton of tropical intraseasonal oscillations. *Proc. Natl. Acad. Sci. USA,* **106,** 8417–8422.

Mekonnen, A., C. D. Thorncroft, A. R. Aiyyer, and G. N. Kiladis, 2008: Convectively coupled Kelvin waves over tropical Africa during the boreal summer: Structure and variability. *J. Climate,* **21,** 6649–6667.

Mounier, F., G. N. Kiladis, and S. Janicot, 2007: Analysis of the dominant mode of convectively coupled Kelvin waves in the West African monsoon. *J. Climate,* **20,** 1487–1503.

Nakazawa, T., 1988: Tropical super clusters within intraseasonal variation over the western Pacific. *J. Meteor. Soc. Japan,* **66,** 823–839.

Nguyen, H., and J.-P. Duvel, 2008: Synoptic wave perturbations and convective systems over equatorial Africa. *J. Climate,* **21,** 6372–6388.

Numaguti, A., R. Oki, K. Nakamura, K. Tsuboki, N. Misawa, T. Aisai, and Y.-M. Kodama, 1995: 4–5-day-period variation and low level dry air observed in the equatorial western Pacific during the TOGA-COARE IOP. *J. Meteor. Soc. Japan,* **73,** 267–290.

Rashid, H. A., H. H. Hendon, M. C. Wheeler, and O. Alves, 2011: Prediction of the Madden–Julian oscillation with the POAMA dynamical prediction system. *Climate Dyn.,* **36,** 649–661, doi:10.1007/s00382-010-0754-x.

Ridout, J. A., and M. K. Flatau, 2011: Convectively coupled Kelvin wave propagation past Sumatra: A June case and corresponding composite analysis. *J. Geophys. Res.,* **116,** D07106, doi:10.1029/2010JD014981.

Roundy, P. E., 2008: Analysis of convectively coupled Kelvin waves in the Indian Ocean MJO. *J. Atmos. Sci.,* **65,** 1342–1359.

——, 2012: Observed structure of convectively coupled waves as a function of equivalent depth: Kelvin waves and the Madden–Julian oscillation. *J. Atmos. Sci.,* **69,** 2097–2106.

——, and W. M. Frank, 2004: A climatology of waves in the equatorial region. *J. Atmos. Sci.,* **61,** 2105–2132.

Sherwood, S. C., 1999: Convective precursors and predictability in the tropical west Pacific. *Mon. Wea. Rev.,* **127,** 2977–2991.

——, and R. Wahrlich, 1999: Observed evolution of tropical deep convective events and their environment. *Mon. Wea. Rev.,* **127,** 1777–1795.

Sobel, A. H., and D. Kim, 2012: The MJO-Kelvin wave transition. *Geophys. Res. Lett.,* **39,** L20808, doi:10.1029/2012GL053380.

——, S. E. Yuter, C. S. Bretherton, and G. N. Kiladis, 2004: Large-scale meteorology and deep convection during TRMM KWAJEX. *Mon. Wea. Rev.,* **132,** 422–444.

Straub, K. H., and G. N. Kiladis, 2003a: Interactions between the boreal summer intraseasonal oscillation and higher frequency tropical wave activity. *Mon. Wea. Rev.,* **131,** 945–960.

——, and ——, 2003b: The observed structure of convectively coupled Kelvin waves: Comparison with simple models of coupled wave instability. *J. Atmos. Sci.,* **60,** 1655–1668.

Takayabu, Y. N., 1994: Large-scale cloud disturbances associated with equatorial waves. Part I: Spectral features of the cloud disturbances. *J. Meteor. Soc. Japan,* **72,** 433–448.

——, and M. Murakami, 1991: The structure of super cloud clusters observed in 1–20 June 1986 and their relationship to easterly waves. *J. Meteor. Soc. Japan,* **69,** 105–125.

Thayer-Calder, K., and D. A. Randall, 2009: The role of convective moistening in the Madden–Julian oscillation. *J. Atmos. Sci.,* **66,** 3297–3312.

Ushiyama, T., S. Satoh, and K. Takeuchi, 1995: Time and spatial variations of mesoscale rainfalls and their relation to the large-scale field in the western tropical Pacific. *J. Meteor. Soc. Japan,* **73,** 379–392.

Ventrice, M. J., C. D. Thorncroft, and M. A. Janiga, 2012a: Atlantic tropical cyclogenesis: A three-way interaction between an African easterly wave, diurnally varying convection, and a convectively coupled atmospheric Kelvin wave. *Mon. Wea. Rev.,* **140,** 1108–1124.

——, ——, and C. J. Schreck III, 2012b: Impacts of convectively coupled Kelvin waves on environmental conditions for Atlantic tropical cyclogenesis. *Mon. Wea. Rev.,* **140,** 2198–2214.

Vitart, F., and F. Molteni, 2010: Simulation of the Madden–Julian Oscillation and its teleconnections in the ECMWF forecast system. *Quart. J. Roy. Meteor. Soc.,* **136,** 842–855, doi:10.1002/Qj.623.

Waliser, D. E., 2006: Intraseasonal variations. *The Asian Monsoon,* B. Wang, Ed., Springer, 787 pp.

——, 2011: Predictability and forecasting. *Intraseasonal Variability of the Atmosphere-Ocean Climate System,* 2nd ed. W. K.-M. Lau and D. E. Waliser, Eds., Springer, 433–476.

Wang, B., 1988: Dynamics of tropical low-frequency waves: An analysis of the moist Kelvin wave. *J. Atmos. Sci.,* **45,** 2051–2065.

Wang, H., and R. Fu, 2007: The influence of Amazon rainfall on the Atlantic ITCZ through convectively coupled Kelvin waves. *J. Climate,* **20,** 1188–1201.

Wheeler, M., and G. N. Kiladis, 1999: Convectively coupled equatorial waves: Analysis of clouds and temperature in the wavenumber–frequency domain. *J. Atmos. Sci.,* **56,** 374–399.

——, and H. H. Hendon, 2004: An all-season real-time multivariate MJO index: Development of an index for monitoring and prediction. *Mon. Wea. Rev.,* **132,** 1917–1932.

——, G. N. Kiladis, and P. J. Webster, 2000: Large-scale dynamical fields associated with convectively coupled equatorial waves. *J. Atmos. Sci.,* **57,** 613–640.

Wu, X., and M. A. LeMone, 1999: Fine structure of cloud patterns within the intraseasonal oscillation during TOGA COARE. *Mon. Wea. Rev.,* **127,** 2503–2513.

Zhang, C., 2005: The Madden-Julian oscillation. *Rev. Geophys.,* **43,** RG2003, doi:10.1029/2004RG000158.

Zhang, M. H., and M. A. Geller, 1994: Selective excitation of tropical atmospheric waves in wave-CISK: Effect of vertical wind shear. *J. Atmos. Sci.,* **51,** 353–368.

Zhu, H. Y., H. Hendon, and C. Jakob, 2009: Convection in a parameterized and superparameterized model and its role in the representation of the MJO. *J. Atmos. Sci.,* **66,** 2796–2811.